



# Production of CO<sub>2</sub>-neutral liquid fuels by integrating Fischer-Tropsch synthesis and hydrocracking in a single micro-structured reactor: Performance evaluation of different configurations by factorial design experiments



Hannah Kirsch\*, Natalie Lochmahr, Christiane Staudt, Peter Pfeifer, Roland Dittmeyer

Institute for Micro Process Engineering, Karlsruhe Institute of Technology, Hermann-von-Helmholtz-Platz 1, Eggenstein-Leopoldshafen D-76344, Germany

## HIGHLIGHTS

- Process intensification by integrating Fischer-Tropsch Synthesis and Hydrocracking.
- Performance study of integrated process by factorial design experiments.
- Product characteristics strongly influenced by the integration configuration.
- Suggestion of elaborated integration patterns of both reactions.
- Practical application of Power-to-Liquid process feasible.

## ARTICLE INFO

### Keywords:

Fischer-Tropsch synthesis  
Hydrocracking  
Power-to-Liquid  
Synthetic fuels  
Process integration  
Micro-structured reactor

## ABSTRACT

Humankind must drastically reduce CO<sub>2</sub> emissions within the next three decades to limit global climate change. Defossilization of the transport sector must contribute to the achievement of this ambitious aim. One promising option is the production of synthetic liquid fuels from CO<sub>2</sub>, water, and renewable electrical energy. Liquid fuels will also be used in the future, especially for heavy-duty vehicles and aviation. We studied the production of liquid fuels by integration of Fischer-Tropsch Synthesis (FTS) and Hydrocracking (HC) in a single micro-structured reactor. Thereby, we addressed the aspects of process simplification and process intensification. Both are particularly important for flexible small-scale plants for decentralized application in context of the energy transition. In this study, we systematically investigated the performance of the integrated FTS/HC process depending on different operating conditions (pressure, temperature, weight hourly space velocity, H<sub>2</sub>/CO synthesis gas ratio) and integration configurations by applying a factorial design approach. Beyond the selectivity of the process towards liquid fuels, we especially focus on the product quality affected by the type of produced hydrocarbons. We identified significant influence parameters on process performance, which is essential to know for practical application. We showed that the crude product quality was significantly influenced by the integration pattern. Therefore, we suggested more elaborate integration configurations to overcome the challenge of suboptimal operation conditions for the FT and HC catalyst and improve the product quality.

## 1. Introduction

Climate change is a global concern. Its consequences – such as desertification, melting of polar ice caps, rising sea levels, and the occurrence of extreme weather events – threaten the livelihoods and welfare of humankind [1]. From local to national scales, governments across the world have therefore committed themselves to drastically reduce anthropogenic greenhouse gas emissions, in particular CO<sub>2</sub>

emissions [2–5]. The so-called 1.5 °C report by the International Panel on Climate Change (IPCC) sets the ambitious aim to reach net zero CO<sub>2</sub> emissions by 2050 [3]. The transport sector is responsible for about 23 percent of global CO<sub>2</sub> emissions [6]. However, globally, little success was achieved in reducing CO<sub>2</sub> emissions in the transport sector in recent years, and the share of renewable energies has stagnated around 3 percent [6].

Liquid fuels will most likely continue to play an important role in

\* Corresponding author.

E-mail address: [hannah.kirsch@kit.edu](mailto:hannah.kirsch@kit.edu) (H. Kirsch).

<https://doi.org/10.1016/j.cej.2020.124553>

Received 18 December 2019; Received in revised form 11 February 2020; Accepted 21 February 2020

Available online 22 February 2020

1385-8947/ © 2020 The Authors. Published by Elsevier B.V. This is an open access article under the CC BY-NC-ND license (<http://creativecommons.org/licenses/by-nc-nd/4.0/>).

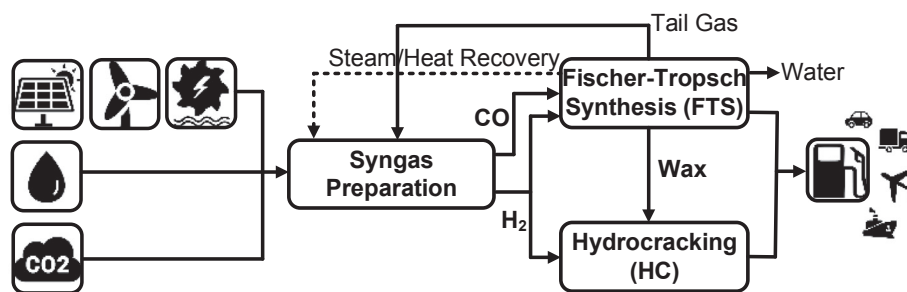
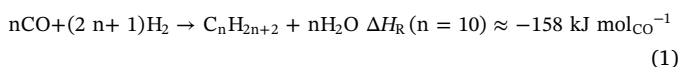


Fig. 1. Exemplary PtL process based on FTS and HC. CO<sub>2</sub>-neutral synthetic liquid fuels are synthesized from CO<sub>2</sub>, water, and renewable electrical energy.

transportation alongside other concepts such as electric mobility, especially for heavy duty vehicles and aviation [7]. So-called Power-to-Liquid (PtL) processes produce synthetic liquid fuels from CO<sub>2</sub> and water using renewable electrical energy. The CO<sub>2</sub> can be obtained from industrial exhaust gases, which cannot be avoided. Moreover, it is possible to create a carbon dioxide neutral cycle if CO<sub>2</sub> is filtered directly from the air by direct air capture [8,9] or captured from biogas [10,11]. The first process step produces synthesis gas (hereafter referred to as syngas), a mixture of hydrogen and carbon monoxide. There are several methods to produce syngas, such as electrolysis in combination with reverse water-gas-shift reaction [12], or co-electrolysis [13]. A promising subsequent approach to convert syngas into liquid fuels is the combination of the Fischer-Tropsch Synthesis (FTS) and Hydrocracking (HC) to produce middle distillates (potential synthetic Kerosene and Diesel substitutes). The produced synthetic fuel may still need further processing due to fuel quality regulations in place for blending or even direct use. This could be done in existing refineries or eventually on site in a fuel upgrading module. This is a topic of research and development in ongoing projects. Fig. 1 illustrates an exemplary PtL process based on FTS and HC.

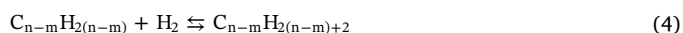
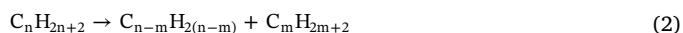
FTS is a highly exothermic reaction, which delivers a wide range of hydrocarbons of different chain length depending on the reaction conditions and the catalyst. The cobalt-catalyzed FTS at low temperature, i.e. 200–250 °C, produces mainly linear saturated hydrocarbons (eq. (1)) [14].



However, as the FTS is subject to polymerization kinetics, the maximum selectivity towards the desired middle distillate fraction is limited and the formation of long chain hydrocarbons cannot be avoided [15]. The Anderson-Schulz-Flory distribution (ASF) describes in first approximation the product distribution of the FTS. According to the ASF, the C<sub>10</sub>-C<sub>20</sub> selectivity can reach a maximum value of nearly 40 percent for a chain growth probability of 0.87. The chain growth probability is a function of the catalyst and the reaction conditions. It reflects the ratio between the probability of intermediate desorption and further chain growth.

HC should selectively crack the long chain hydrocarbons produced in the FTS under a hydrogen atmosphere into shorter hydrocarbons (eq. (2)) and saturate the cracking products by hydrogenation (eq. (4)). Cracking of smaller compounds and especially the middle distillate fraction should be avoided in the process. In this way, the selectivity of the overall process towards the desired middle chain hydrocarbons increases, and at the same time the selectivity to gaseous products is minimized. Cracking is always accompanied by isomerization (eq. (3)), which improves the cold flow properties of the fuel [14]. For HC, a bifunctional metallic and acidic catalyst is used [16]. The metal sites catalyze hydrogenation and dehydrogenation. At the Brønsted acid sites, skeletal rearrangements and scissions of the carbon-carbon bonds take place. The widespread mechanistic view [16] is that HC occurs via alkenes and carbocations occur as intermediates. Saturated

hydrocarbons produced in the FTS are dehydrogenated to alkenes at the metal site. The alkenes are further converted on the acid site via isomerization and cracking into shorter saturated and unsaturated hydrocarbons. The olefinic cracking products can be converted on the metal via further hydrogenation. If pure primary hydrocracking without multiple cracking of hydrocarbons occurs, it is called ideal hydrocracking [16].



Electricity from wind and solar energy, which are the most promising renewable sources, is subject to strong fluctuations in the time of day and season. Moreover, there could be a discrepancy between the place of generation and the place of demand as renewable energy is generated more locally than energy from conventional sources. This local energy production suggests compact, small-scale, container-based plants, easily installable next to the energy source [17]. For these compact plants, the number of process steps must be minimized to reduce CAPEX without losing process efficiency. Besides, processes commercially operated on large-scale cannot be implemented economically on small-scale. Thus both, process simplification and process intensification become very important.

To simplify the process, FTS and HC can be integrated. Integration can take place on different scales, ranging from the level of the catalyst active site to the level of process design [18]. Newly developed catalysts open up integration at the catalyst level by combining the catalyst functions for FTS and HC [19–23]. Integration on reactor level is achieved by arranging both catalysts in a single reactor [24–28]. This paper focuses on integration at the reactor level. To address the aspect of process intensification, we use a micro-structured reactor. Micro-structured reactors have a large volumetric surface area resulting in excellent heat and mass transfer properties for FTS [29,30]. Hence, high conversion rates per reactor volume as well as high per-pass yield can be achieved, even with highly active catalysts. Dynamic operation of the micro-structured reactor is also feasible [31]. So-called numbering-up can considerably facilitate scale-up [32]. One of the challenges for integrating FTS and HC in one reactor is that both catalysts need to operate under the same, usually suboptimal, reaction conditions [33,34].

This experimental study investigates the performance of an integrated FTS/HC-process in a micro-structured reactor accounting for various integration patterns as well as different operation conditions such as pressure, temperature, weight hourly space velocity (WHSV), and H<sub>2</sub>/CO syngas ratio. We report the effects of the operating conditions on the conversion, product distribution, as well as the product quality. Going beyond existing studies in literature [28], we do not only analyze the chain length distribution of the produced hydrocarbons, but we also look at the type of produced hydrocarbons distinguishing between n-alkanes, iso-alkanes, and olefins. The type of produced hydrocarbons decisively influences the quality of the product. For a

comprehensive evaluation of the integrated FTS/HC process in a single reactor, the analysis of the type of produced hydrocarbons is particularly interesting, as for example the presence of CO during hydrocracking is known to affect production of olefins [33,34]. In comparison to other literature studies, applying the method of design of experiments with a complete second order factorial design allows the systematic and unbiased examination of the influence of the considered factors independently from each other. In particular, statistical experiment planning is useful to avoid misinterpretation of experimental data through slight catalyst deactivation over the time of experiments. We define significant process factors for the defined target values. Moreover, we identify the level of each factor that is favorable for each target value. The use of factorial design experiments allows considerable reduction of the number of individual test points without losing important information. The interpretation of results focuses on the practical application in PtL plants and is of widespread significance.

## 2. Experimental design

### 2.1. Catalyst preparation

We prepared two catalysts by incipient wetness impregnation following Ref. [28]. The Fischer-Tropsch (FT)-catalyst consists of 20 wt% Co and 0.5 wt% Re as promoter supported on  $\gamma$ -Al<sub>2</sub>O<sub>3</sub>. The  $\gamma$ -Al<sub>2</sub>O<sub>3</sub> support (3  $\mu$ m, 80–120 m<sup>2</sup>/g, Alfa Aesar) was impregnated with an aqueous precursor solution containing cobalt(II)nitrate hexahydrate (Sigma-Aldrich) and perrhenic acid (75–80 wt% aq. soln., Alfa Aesar). After drying overnight at 120 °C, the catalyst was calcined in air at 400 °C for 2 h.

HC-catalyst Pt-ZSM5 with 0.5 wt% Pt was used. NH<sub>4</sub>-ZSM5 (425 m<sup>2</sup>/g, 80:1 mol ratio SiO<sub>2</sub>:Al<sub>2</sub>O<sub>3</sub>, Alfa Aesar) was calcined at 550 °C for 12 h to form H-ZSM5. H-ZSM5 was impregnated with an aqueous precursor solution containing tetraammineplatinum(II) hydroxide solution (8–11 wt% Pt, Alfa Aesar). After drying overnight at 120 °C, the catalyst was calcined in air at 550 °C for 6 h.

The weight percentages of the metals reflect the elemental metal content in the reduced catalyst. For more information on the catalysts, see Table 1. Deviations between the nominal values of the metal content and actual ones are mainly due to errors in dosing and weighing when producing small batches of catalyst. Both, FT and HC catalyst were pressed into tablets and crushed to small particles avoiding large pressure drop. For the experiments, we used a sieve fraction with a mesh of 50 – 100  $\mu$ m. Prior to the experiments, the catalysts were reduced in situ in a hydrogen flow with WHSV 2 h<sup>-1</sup> at ambient pressure and 340 °C (temperature ramp of 1 °C/min and dwell time of 15 h).

### 2.2. Experimental setup

We carried out the experiments in an oil-cooled micro fixed-bed reactor allowing near-isothermal operation. The reactor has a total catalyst bed volume of 6.8 cm<sup>3</sup> and the catalyst is filled into a 1.5 mm

wide annular gap (Fig. 2a). We studied two different catalyst bed configurations (Fig. 2b). In the case of the sequential configuration, the FT catalyst and HC catalyst were arranged in series. In the case of the hybrid configuration, the catalyst bed consisted of a well-blended physical mixture of FT and HC catalyst. We loaded equal masses of each catalyst (0.8 g) into the reactor, following previous studies [28]. The catalysts were diluted with inert  $\alpha$ -Al<sub>2</sub>O<sub>3</sub>. For the corresponding FT reference experiments, the HC catalyst was replaced with inert material and the catalyst bed contained only FT catalyst mixed with  $\alpha$ -Al<sub>2</sub>O<sub>3</sub>. Thus, the length of the FT catalyst bed was identical to those of the integrated FTS/HC experiments. In comparison to the sequential order, the FT catalyst was distributed over the FT bed length. In comparison to the hybrid bed, the FT catalyst was distributed over the whole bed length.

Fig. 3 shows a simplified flow scheme of the test rig. H<sub>2</sub>, CO and N<sub>2</sub> were dosed by mass flow controllers (MFC). Synthesis gas was diluted with 3 vol% nitrogen as internal standard for the gas chromatograph (GC) measurements. Most of the incoming gas flow was preheated to 200 °C and passed through the reactor. A small part of the gas flow bypassed the reactor allowing measurement of the composition of the reactant flow. The product stream leaving the reactor was separated in the hot trap, operated at 190 °C, and then in the cold trap, which is cooled to 6 °C. In the hot trap, we collected the wax fraction. In the cold trap, we condensed the liquid fraction and the by-product water. The remaining permanent gases were injected into an online-GC. The compositions of the wax and the liquid product samples were analyzed in an offline-GC. A back pressure regulator valve maintained a constant pressure at a defined level in the system.

We ran experiments up to 1100 h on stream. After a running-in phase of 200–300 h, we started the test points. We maintained the process conditions of each test point for about 24 h, and we collected steady state samples during the last 12–15 h of each point.

### 2.3. Product analysis

The gaseous products were analyzed by an online-GC (Agilent 6890 N). It is equipped with two columns: a molecular sieve 19095P-MS6 to separate the permanent gases H<sub>2</sub>, CO, N<sub>2</sub>, CH<sub>4</sub>, and a HP-Plot/Q 19095P-Q04 for the separation of the hydrocarbons C<sub>2</sub>-C<sub>7</sub>. A thermal conductivity detector (TCD) or a flame ionization detector (FID), respectively quantified all gases. The TCD measures the permanent gases H<sub>2</sub>, CO, N<sub>2</sub> and CH<sub>4</sub>. The FID quantifies all hydrocarbons by combustion in a hydrogen flame.

The liquid phase from the cold trap was separated into an aqueous phase and an oily phase containing liquid hydrocarbons. The oil phase was analyzed in an offline-GC (Agilent 7820A) with an autoinjector equipped with a DB-2887 column and a FID. The wax phase from the hot trap was dissolved in carbon disulfide (CS<sub>2</sub>) and analyzed in an offline-GC (Agilent G1530A) equipped with a heated injector module (Gerstel KAS cold feed system with controller C506), the column MXT-1HT, and a FID.

**Table 1**

Physical properties of the self-prepared FT and HC catalyst. For FTS we used a Co/Re-Al<sub>2</sub>O<sub>3</sub> catalyst; for HC we used a Pt-ZSM5 catalyst. We characterized both catalysts after calcination, before reduction.

catalyst	composition <sup>a</sup> (wt%)	surface area <sup>b</sup> (m <sup>2</sup> /g)	metal dispersion <sup>c</sup> (%)
Co/Re-Al <sub>2</sub> O <sub>3</sub>	Co 17.9 ± 5.2, Re 0.9 ± 0.3	95 ± 4	4.9
Pt-ZSM5	Pt 0.4 ± 0.006	(447 ± 4)	2.8

<sup>a</sup> Metal content was quantified by ICP (inductively coupled plasma) measurements. Indicated value is mean value of three repeated analysis.

<sup>b</sup> Surface areas were determined on a Micromeritics 3Flex by nitrogen physisorption at 77 K and calculated after BET (Brunauer, Emmett and Teller)-method [35]. Indicated value is mean value of five repeated analysis. Surface areas for HC catalyst in brackets as the applicability of the BET equation for the analysis of microporous materials such as zeolites is limited in a strict sense, see [59].

<sup>c</sup> Metal dispersions were determined on a Micromeritics 3Flex by hydrogen chemisorption. After online reduction of the catalyst at 350 °C for 15 h with a temperature ramp of 2 °C/min in a 5 percent H<sub>2</sub>/Ar flow followed by an evacuation of 30 min, the measurement was performed at 35 °C. Metal dispersion is calculated according to Ref. [36].

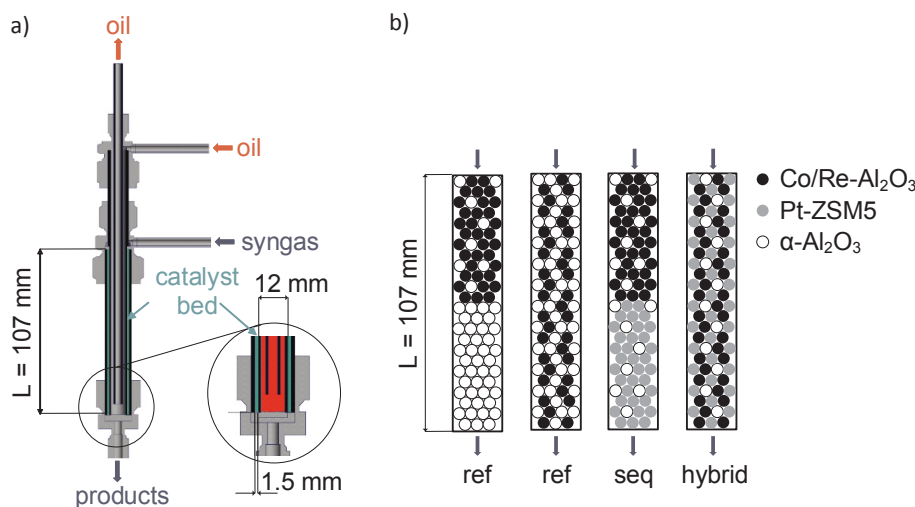


**Fig. 2.** a. Micro fixed-bed reactor used in the experiments. The catalyst bed consists of a 1.5 mm wide annular gap. Oil-cooling allows quasi-isothermal operation. b. Catalyst configurations for FT reference experiments (ref) and integrated FTS/HC experiments (seq) FT and HC catalyst were arranged in series; in the hybrid configuration (hybrid) both catalysts were physically mixed. We used equal mass (0.8 g) of each catalyst. The catalysts were diluted with inert  $\alpha$ -Al<sub>2</sub>O<sub>3</sub>. Two FT reference experiments (ref) were applied for comparison with the sequential and hybrid bed, where we replaced the HC catalyst with  $\alpha$ -Al<sub>2</sub>O<sub>3</sub>.

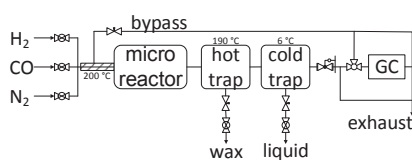


**Fig. 3.** Simplified flow scheme of the test rig. The reactants H<sub>2</sub>, CO and N<sub>2</sub> were mixed, preheated and fed into the micro-structured reactor. In the reactor, both reactions, FTS and HC, were integrated. The products were separated by a hot trap and a cold trap and analyzed by gas chromatography.

The integral mass flow of the liquid and the wax phase was determined for more than 12 h under steady-state conditions. The total mass balance and atomic closures were typically better than  $\pm 10\%$ . According to experience, the main error source is the collection of liquid and wax phase from the traps. Residues of wax and oil could remain in the two traps. Furthermore, releasing the samples to ambient pressure for analysis causes short chain hydrocarbons, originally dissolved in the liquid and wax phase, to escape. The separation of hydrocarbons and water is another error source. The closure of the mass balance affects the selectivities, while the relative error is less than 11 percent.

We calculated the CO conversion  $X_{CO}$  and the carbon monoxide-related integral selectivity  $Y_{i,CO}$  of the hydrocarbons according to the following equations:

$$X_{CO} = \frac{\dot{N}_{CO,in} - \dot{N}_{CO,out}}{\dot{N}_{CO,in}} \quad (5)$$

where  $\dot{N}$  is the molar flow rate; in and out refer to the inlet and outlet of the reactor respectively.

$$Y_{i,CO} = \frac{\dot{N}_{i,out}}{\dot{N}_{CO,in} - \dot{N}_{CO,out}} \times n_{c,i} \quad (6)$$

where  $\dot{N}_i$  is the molar flow rate of hydrocarbon  $i$ ,  $n_{c,i}$  is the carbon number of hydrocarbon  $i$ .

We classified the hydrocarbon products into lumps sums according to the C number: C<sub>1</sub>-C<sub>9</sub>, C<sub>10</sub>-C<sub>20</sub> and C<sub>21</sub>+. Furthermore, we distinguished between n-alkanes, isomers, and alkenes. No aromatics could be detected.

#### 2.4. Experimental design

We conducted the experiments following an approach of statistical design of experiments [37,38]. In statistical design of experiments, target values, factors, and factor levels are defined. Target values are

measured quantities or quantities calculated from measured values, which describe the experiment result. Factors are the presumed significant influence parameters on the defined target values. The values that the factors take on in the experiments are called levels. If an experiment design contains many factors, normally two levels for each factor are considered to limit the effort. This results in a factorial experiment design designated as (number of levels)<sup>(number of factors)</sup>. We investigated the effect of the process conditions pressure, temperature, WHSV, and H<sub>2</sub>/CO syngas ratio by a complete 2<sup>4</sup> factorial design. The WHSV was related to the FT catalyst mass. As target values, we defined the CO conversion, the C<sub>10</sub>-C<sub>20</sub> selectivity and the isomer selectivity. We aimed to maximize all target values. A triple repetition of a center point allowed identification of possible time-dependent effects and testing of the reproducibility of the experiments. The operating conditions ranged the following:  $p = 20$ –30 bar,  $T = 225$ –255 °C,  $WHSV = 6$ –12 h<sup>-1</sup>, and H<sub>2</sub>/CO syngas ratio = 1.7–2.2. The center point was located equidistant from the two levels of the test point. The levels are coded with -1, 0, and 1 (Table 2). Table 3 shows the experiment factorial design with 19 points in total (16 test points and 3 center points). For the experiments, we randomized the order of the test points.

We calculated the effect of a factor on the defined target values as described in literature for experiment design [37]. Applying a complete 2<sup>4</sup> factorial design, for each factor, there are eight pairs of experiments where only the considered factor differs, and all other three factors are the same. For example, for the factor pressure, the experiment pairs are the following: 3/11, 7/12, 6/4, 10/2, 8/15, 5/13, 9/14, 1/16. The difference in the target values of these experiment pairs is a measure of the effect of the factor. We obtained the effects by the calculation of the mean value of these differences.

$$E_{x,y} = \frac{2}{m} \times \sum_{n=1}^m y_n \times \text{sgn}(x_n) \quad (7)$$

where  $E_{x,y}$  is the effect of factor  $x$  on target value  $y$ ,  $m$  is the number of test points,  $\text{sgn}$  is the signum function to extract the level (-1 or +1) of

**Table 2**

Level coding of the factors (influence parameters) for factorial experiment design. We accounted for four factors: pressure, temperature, WHSV, and H<sub>2</sub>/CO syngas ratio. We defined two levels for each factor: lower level (-1), upper level (+1), level 0 refers to the center point.

level	pressure/bar	temperature/°C	WHSV/h <sup>-1</sup>	H <sub>2</sub> /CO ratio/-
-1	20	225	6	1.7
0	25	240	9	1.95
+1	30	255	12	2.2

**Table 3**

Complete  $2^4$  factorial experiment design with 16 test points. We extended the  $2^4$  factorial design with triple repetition of a center point. For the level coding of the factors, please refer to Table 2.

Point	pressure	temperature	WHSV	H <sub>2</sub> /CO ratio
center	0	0	0	0
3	-1	-1	-1	-1
11	+1	-1	-1	-1
7	-1	+1	-1	-1
12	+1	+1	-1	-1
6	-1	-1	+1	-1
4	+1	-1	+1	-1
10	-1	+1	+1	-1
2	+1	+1	+1	-1
center	0	0	0	0
8	-1	-1	-1	+1
15	+1	-1	-1	+1
5	-1	+1	-1	+1
13	+1	+1	-1	+1
9	-1	-1	+1	+1
14	+1	-1	+1	+1
1	-1	+1	+1	+1
16	+1	+1	+1	+1
center	0	0	0	0

the factor.

The absolute value of the effects is a measure of how strongly the factor influences the target value. In case of positive effects, factor and target value are positively correlated. In case of negative effects, factor and target value are negatively correlated. It should be noted that in case of small influence of a factor on a target value, the difference in the target values of the individual experiment pairs can differ in sign, and hence, the calculated effect is not significant.

### 3. Results and discussion

#### 3.1. Study of the FT reference

##### 3.1.1. Effect of operating conditions on conversion and selectivity

We conducted FT experiments as reference for the integration of FTS and HC. We did not observe significant differences between the two FT reference experiments with different catalyst bed configurations (Appendix, Fig. 8). Consequently, we do not distinguish between these two experiments in the following, but mentioning only “FT reference experiment”. As previously mentioned, we investigated the effect of pressure, temperature, WHSV, and H<sub>2</sub>/CO syngas ratio on the CO conversion, C<sub>10</sub>-C<sub>20</sub> selectivity and isomer selectivity. Table 4 lists the overall effects. The catalyst deactivated over the time of the experiments (see measured CO conversion of center points Z1, Z2, Z3 in Fig. 4 highlighted in red). We corrected the measured CO conversion in order to obtain a time-independent effect of the input parameters on the CO

**Table 4**

Overall maximum factor for the effect of pressure, temperature, WHSV, and H<sub>2</sub>/CO syngas ratio on CO conversion, C<sub>10</sub>-C<sub>20</sub> selectivity, and isomer selectivity for the FT reference experiment. The absolute value of the effects is a measure of how strongly the factors influence the target values. In case of a positive effect, factor and target value are positively correlated. In case of a negative effect, factor and target value are negatively correlated. For calculation of the effects, please refer to section 2.4.

	CO conversion	C <sub>10</sub> -C <sub>20</sub> selectivity	Isomer selectivity
pressure	0.81%*	-1.44%	-1.09%
temperature	28.67%*	11.67%	0.26%
WHSV	-12.46%*	-4.39%	-0.43%
H <sub>2</sub> /CO ratio	6.18%*	-0.60%	-0.22%

\* Corrected CO conversion taking into account catalyst deactivation (see section 3.1.3).

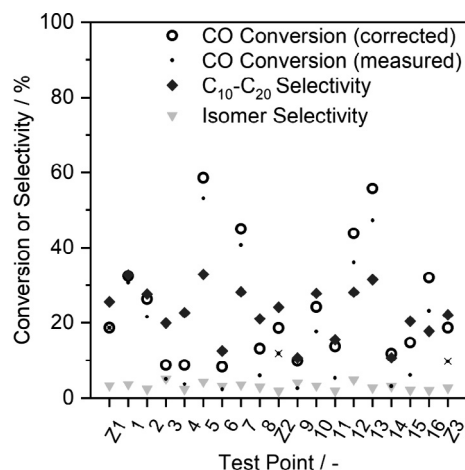


**Fig. 4.** CO conversion (corrected and measured), C<sub>10</sub>-C<sub>20</sub> selectivity, and isomer selectivity for all test points of the FT reference experiments. Z1, Z2 and Z3 refer to the center points. For the operating conditions of each test point, please refer to Table 2 and Table 3. For the correction of the CO conversion, please refer to section 3.1.3. The measured CO conversions of the three center points (marked with a cross) are a measure for the deactivation of the FT catalyst during the experiments.

conversion. For more information, see section 3.1.3.

The CO conversion reaches up to 60 percent (Fig. 4). Of the presumed factors, temperature most affects the CO conversion, followed by WHSV, H<sub>2</sub>/CO syngas ratio, and pressure (Table 4). The C<sub>10</sub>-C<sub>20</sub> selectivity ranges from 10 to 35 percent (Fig. 4). The influence of temperature on the C<sub>10</sub>-C<sub>20</sub> selectivity is the strongest, followed by WHSV, pressure, and H<sub>2</sub>/CO syngas ratio (Table 4). The isomer selectivity is lower than 5 percent (Fig. 4). No input parameter shows a distinctive effect on the isomer selectivity (Table 4). Though not part of the discussion, information about the C<sub>1</sub>-C<sub>9</sub> selectivity and the C<sub>21+</sub> selectivity are provided in the Supplementary Information.

Temperature rise leads to increased CO conversion due to the exponential increase of the reaction rate with temperature according to Arrhenius law. Besides, a higher temperature favors the endothermic desorption process of the products from the catalyst surface resulting in a lower chain growth probability. The here observed positive correlation of the temperature on the C<sub>10</sub>-C<sub>20</sub> selectivity indicates that at a temperature of 225 C the chain growth probability is at high values where more hydrocarbons with more than 20 C-atoms are formed. With increasing temperature the product spectrum of the FTS is shifted towards shorter hydrocarbons and more hydrocarbons in the range of 10–20 C-atoms are produced. But the selectivity towards gaseous products also increases.

An increased WHSV corresponds to a reduced residence time of the reactants in the reactor. Consequently, the probability of chain initiation and chain growth reactions drops, and CO conversion decreases. Lower CO conversion coincides with lower C<sub>10</sub>-C<sub>20</sub> selectivity. With rising CO conversion, the H<sub>2</sub>/CO ratio decreases as the usage ratio of the FTS is above two. Lower H<sub>2</sub>/CO ratio results in higher CO concentration on the catalyst surface promoting chain growth.

Higher total pressure results in improved CO conversion due to the increase of the reaction rate with higher partial pressure of the reactants. The chain growth is promoted with elevated pressure since CO adsorbs more strongly on the catalyst surface and, hence, the possibility of further carbon integration into the chain increases. The here observed negative correlation of the pressure on the C<sub>10</sub>-C<sub>20</sub> selectivity indicates that at a total pressure of 30 bar the chain growth probability shifted to values where more hydrocarbons with more than 20 C-atoms are formed.

The effect of the H<sub>2</sub>/CO syngas ratio on CO conversion and C<sub>10</sub>-C<sub>20</sub> selectivity is more complex as it depends on the usage ratio during

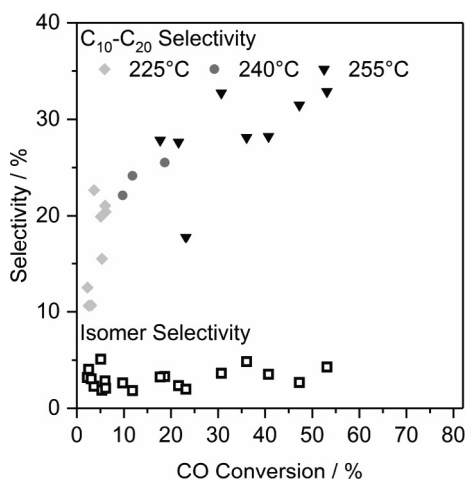


Fig. 5. C<sub>10</sub>-C<sub>20</sub> selectivity and isomer selectivity over the CO conversion for all test points of the FT reference experiments. Data is plotted over the original measured CO conversion.

synthesis, which is in itself dependent on CO conversion and selectivity. The usage ratio is the ratio of the reaction rates of H<sub>2</sub> and CO. Producing infinitely long carbon chains, the usage ratio approaches two. The usage ratio is influenced by the H<sub>2</sub>/CO syngas ratio. An understoichiometric H<sub>2</sub>/CO syngas ratio limits CO conversion. In general, with higher H<sub>2</sub>/CO ratio the driving force for hydrogenation becomes stronger and the chain growth probability decreases. Under the conditions applied, the C<sub>10</sub>-C<sub>20</sub> selectivity declines with higher H<sub>2</sub>/CO ratio indicating that the product spectrum is shifted towards hydrocarbons with less than 20 C-atoms. Nevertheless, under specific conditions starting at high alpha values and thus high C<sub>21+</sub> selectivity, an increase in the C<sub>10</sub>-C<sub>20</sub> selectivity could also happen.

### 3.1.2. Effect of CO conversion on selectivity

Fig. 5 shows the C<sub>10</sub>-C<sub>20</sub> selectivity and isomer selectivity as a function of the measured CO conversion for the FT reference experiments. The isomer selectivity seems to be independent of the CO conversion, whereas the C<sub>10</sub>-C<sub>20</sub> selectivity is strongly correlated with the CO conversion. It should be noted, that when comparing test points operated at the same temperature, a dependence of the C<sub>10</sub>-C<sub>20</sub> selectivity on CO conversion can also be observed. In Fig. 5, the temperature of the corresponding test points is indicated for the C<sub>10</sub>-C<sub>20</sub> selectivity. At a temperature of 225 °C, CO conversion is up to 6 percent; at a temperature of 240 °C, CO conversion ranges from 10 to 19 percent; and at a temperature of 255 °C, CO conversion is between 22 and 53 percent. It should be noted, that when comparing test points operated at the same temperature, a dependence of the C<sub>10</sub>-C<sub>20</sub> selectivity on CO conversion can also be observed. Up to a CO conversion of approx. 30 percent, it seems that the C<sub>10</sub>-C<sub>20</sub> selectivity increases with higher CO conversion (except for one data point). This demonstrates that the chain growth also depends on the CO conversion. This phenomenon is already described elsewhere in literature [31,39–41]. Presumably, water inhibits the hydrogenation of olefins which could then readsorb and contribute to chain growth.

Consequently, the C<sub>10</sub>-C<sub>20</sub> selectivity is not only a function of the operating conditions, but is also a function of conversion in a more complex way.

### 3.1.3. FT catalyst deactivation

The FT catalyst deactivated over the experiment time of approx. 1100 h. The CO conversion dropped with a rate of 0.2 percent absolute value per day, and the total decrease in CO conversion during one experiment never exceeded 10 percent absolute value (see Fig. 4 X<sub>CO</sub>(Z1) = 18.7% and X<sub>CO</sub>(z3) = 9.7%). In all, the FT catalyst shows a

reasonable long-term stability considering the much longer time on stream compared to other studies [28]. Moreover, the fact that the catalyst has been stressed by numerous test points at operation conditions with high temperature and high CO conversion resulting in high water pressure further demonstrates its long-term stability. As mentioned above, we corrected the measured CO conversions to minimize the effect of time-dependencies in our analysis. With the help of the three center points, which we tested at the beginning, at halftime, and at the end of the experiments, we fitted an exponential decline curve (eq. (8)) of the CO conversion over time. In this way, we regarded the CO conversion as a function exclusive of time. We did not consider dependence on other independent variables, such as the process parameters. Within one experiment run, the test points were evenly distributed over the defined ranges of the considered influencing process parameters. This means, that for each process parameter, there are the same number of test points at high level as at low level. Besides, the test points were run for about the same time (~24 h, see section 2.2). Therefore, each test point is weighted equally when calculating a time-dependent deactivation. In reality, deactivation is higher for some test points (e.g. at high temperature) than for others, but the average deactivation over several statistically distributed test points is expected to be similar. Thus, the dependency of CO conversion can most likely be reduced to time on stream. The estimated error of this simplification is a maximum of 5 percent absolute value of CO conversion. Moreover, the activity decrease of the catalyst is exponential over time, which has also been observed in numerous other studies [42–46]. We converted all measured CO conversions to time zero of our experiments. Here, time zero is defined as the time when we started the experiment run with center point Z1 (after the running-in phase, see section 2.2).

$$X_{CO,corrected} = a \cdot e\left(-\frac{t_0}{b}\right) + c \text{ with } c = X_{CO,measured} - a \cdot e\left(-\frac{t}{b}\right) \quad (8)$$

where X<sub>co</sub> is the CO conversion, t is the time starting from Z1, t<sub>0</sub> is the time of Z1, and a, b are constants. The constants a and b are determined by an exponential fit of the CO conversions over experiment time of the three center points (Z1, Z2, and Z3). In case of the FT reference experiment, the constants are: a = 16.3, and b = 254.0. The applicability of the correction of the CO conversion is shown exemplary at one test point in the [Supplementary Information](#).

We observed a stronger catalyst deactivation during test points (Appendix, Fig. 9) with enhanced CO conversion (X<sub>CO</sub> > 30%), regardless of whether the high conversion is due to a high temperature or a low WHSV. This indicates that most likely water as a by-product of the FTS mainly causes the deactivation, which is supported by numerous other studies [47–53].

We did not correct the measured C<sub>10</sub>-C<sub>20</sub> selectivities, which in theory also depend on the CO conversion, due to the complexity of the interrelationships.

## 3.2. Study of the FTS/HC integration

### 3.2.1. Effect of operating conditions on conversion and selectivity

We also investigated the effect of pressure, temperature, WHSV, and H<sub>2</sub>/CO syngas ratio on CO conversion, C<sub>10</sub>-C<sub>20</sub> selectivity, and isomer selectivity for the integrated FTS/HC experiments in both catalyst bed configurations. We evaluated the experiments analogously to the FTS reference experiments. Table 5 summarizes the overall effects.

The CO conversion is primarily determined by the FTS. Hence, we observe the same effects for the integrated FTS/HC experiments as for the FTS reference experiment (Table 4 and Table 5).

For both catalyst bed configurations, of the presumed factors, the influence of temperature on the C<sub>10</sub>-C<sub>20</sub> selectivity is the strongest, followed by WHSV. The influence of pressure and the H<sub>2</sub>/CO syngas ratio on the C<sub>10</sub>-C<sub>20</sub> selectivity is low (Table 5). For the integrated FTS/HC process, the observed effects of the different influencing factors on the target values represent a combination of the individual effects on

**Table 5**

Overall effects of pressure, temperature, WHSV, and H<sub>2</sub>/CO syngas ratio on CO conversion, C<sub>10</sub>-C<sub>20</sub> selectivity, and isomer selectivity for the integrated FTS/HC experiments with both catalyst configurations, the sequential catalyst bed, and the hybrid catalyst bed. The absolute value of the effects is a measure of how strongly the factors influence the target values. In case of a positive effect, factor and target value are positively correlated. In case of a negative effect, factor and target value are negatively correlated. For calculation of the effects, please refer to section 2.4.

	CO conversion		C <sub>10</sub> -C <sub>20</sub> selectivity		Isomer selectivity	
	sequential	hybrid	sequential	hybrid	sequential	hybrid
pressure	3.45%*	4.79%*	2.72%	-0.42%	1.03%	3.64%
temperature	33.51%*	35.84%*	9.40%	6.14%	1.90%	5.33%
WHSV	-16.46%*	-18.67%*	-3.10%	-6.01%	0.33%	2.53%
H <sub>2</sub> /CO ratio	8.00%*	9.55%*	1.28%	2.36%	0.56%	5.16%

\* Corrected CO conversion taking into account catalyst deactivation (see section 3.1.3).

the FTS and on HC, respectively. The individual effects can both have the same sign and amplify each other, or be opposite. In the latter case, the individual effects can weaken each other or one of them clearly outweighs the other one. Moreover, the effects are not only based on the kinetics of FTS and HC, but also on the vapor-liquid equilibrium. The vapor-liquid equilibrium defines the distribution of each component between the vapor and liquid phase. It also determines the volumetric ratio between the two phases influencing the residence time of the liquid phase in the reactor.

Temperature rise leads to an increased C<sub>10</sub>-C<sub>20</sub> selectivity of the integrated process. The FTS produces more hydrocarbons in the range of 10 to 20 C-atoms at elevated temperatures (see section 3.1.1). In addition, the cracking of the long chain hydrocarbons produced by the FTS is also promoted due to several reasons. Firstly, the cracking rate increases exponentially with temperature according to Arrhenius law. Secondly, at higher temperature, dehydrogenation of alkanes to alkenes becomes increasingly easier. Alkenes are cracked more easily according to the HC mechanism. Thirdly, the vapour-liquid equilibrium is affected. With rising temperature, the vapor pressure of the hydrocarbons increases. Then even hydrocarbons of longer chain length occur preferentially in the vapor phase. This results in a decrease of the volume of the liquid phase, and the liquid phase also contains fewer short and middle chain hydrocarbons. Thus, the remaining long chain hydrocarbons in the liquid phase are more selectively cracked. A lower volume flow of liquid phase increases the residence time and thus the fraction of cracked species.

WHSV increase results in a reduced C<sub>10</sub>-C<sub>20</sub> selectivity of the integrated process. As in the case of the FT reference, a high WHSV reduces the total residence time of the reactants over both catalysts reducing the probability for both reactions, FTS and HC, respectively (see section 3.1.1).

The C<sub>10</sub>-C<sub>20</sub> selectivity of the integrated process is increased with rising pressure for the sequential catalyst bed, whereas it is decreased slightly for the hybrid catalyst bed. The FTS produces fewer hydrocarbons in the range of 10 to 20 C-atoms and more long chain hydrocarbons at elevated pressure (see section 3.1.1). This means that, with rising pressure the FTS produces a feed containing more hydrocarbons with more than 20 C-atoms, which then can theoretically be cracked to the desired hydrocarbons in the range of C<sub>10</sub>-C<sub>20</sub>. However, the influence of pressure on hydrocracking is complex. On the one hand, high pressure improves the cracking rate due to increased concentration of long chain hydrocarbons in the liquid phase. On the other hand, elevated pressure diminishes the cracking due to two reasons. First, as in the case of low temperatures, high pressure favors hydrogenation of alkenes to alkanes. Alkanes are cracked less easily according to the HC mechanism. Second, pressure affects the vapor liquid equilibrium. With higher pressure, even shorter hydrocarbons occur preferentially in the liquid phase. The volume of the liquid phase increases, and the liquid phase contains more short hydrocarbons. From the former, a higher volume flow of liquid phase reduces the residence time and thus the fraction of cracked species. From the latter point, the long chain

hydrocarbons are less selectively cracked. Based on these general considerations, we conclude for the case of the sequential bed, that the effect of the FTS producing more long chain hydrocarbons, which can be cracked to hydrocarbons in the range of C<sub>10</sub>-C<sub>20</sub>, along with the effect of rising concentration of the liquid long chain hydrocarbons is dominant. The effects of reduced cracking activity due to a higher alkane concentration and shorter liquid residence time are subordinate. On the contrary, in the case of the hybrid bed, the effect of reduced cracking activity due to higher alkane concentration and shorter liquid residence overweighs the effect of a larger amount of long chain hydrocarbons produced in the FTS. In the hybrid bed, the average vapor/liquid ratio and the average absolute hydrogen partial pressure over the HC catalyst is higher than in the sequential bed, as long chain hydrocarbons are cracked immediately. The higher significance of the reduced cracking activity in the hybrid bed compared to the sequential bed may also be correlated to the fact that a major part of the formed heavy products does not have the same residence time on the HC catalyst in the hybrid bed as in the case of the sequential bed. We performed basic simulation studies which could reproduce the opposite effect of pressure on the sequential and the hybrid bed. However, in the simulation the influence of pressure on the C<sub>10</sub>-C<sub>20</sub> selectivity is considerably lower than observed in the experiments as no vapor-liquid equilibrium is considered. For more information about the simulation, please refer to the [Supplementary Information](#).

A higher H<sub>2</sub>/CO syngas ratio results in an improved C<sub>10</sub>-C<sub>20</sub> selectivity of the integrated process. This effect is opposite as observed in the FT reference experiments. Fewer hydrocarbons in the range of C<sub>10</sub>-C<sub>20</sub> are formed in the FTS (see section 3.1.1). A higher H<sub>2</sub>/CO syngas ratio of the FTS results in a higher H<sub>2</sub>/hydrocarbon ratio for HC. On the one hand, a high H<sub>2</sub>/hydrocarbon ratio reduces the partial pressures of the hydrocarbons and of CO, which promotes hydrogenation of alkenes to alkanes in FT and on the metallic site of HC. Hence, the cracking activity of HC should be decreased. However, the increased ratio of hydrogen hydrocarbons, especially long chain hydrocarbons, seems to be the predominant effect. When taking into account, that the residence time of the liquid phase in the reactor is very likely higher than that of the vapor phase, the ratio of hydrogen to long chain hydrocarbons affects the mass transport between the two phases, and, consequently, the vapor-liquid equilibrium. The higher the hydrogen flow, the higher the partial evaporation of the lighter hydrocarbons from the liquid phase. This leads to a decrease of the volume of the liquid phase, and the liquid phase contains fewer short hydrocarbons. In turn, the long chain hydrocarbons produced in the FTS are more selectively cracked, as observed in the experiments.

All variations of the operation conditions suggest that the isomer selectivity is positively correlated with every input parameters for both integration patterns. However, looking at the individual effect of the related experiment pairs, no clear trend of the effect of pressure, WHSV, or the H<sub>2</sub>/CO syngas ratio on isomer selectivity can be identified. This is shown exemplary for the effect of pressure on the isomer selectivity in the sequential configuration, see [Supplementary Information](#). Only the

positive effect of temperature on isomer selectivity can be confirmed. The isomerization selectivity of the FTS is rather low, regardless of the input parameters. At higher temperatures, the isomerization rate of the HC is accelerated. Moreover, dehydrogenation of alkanes to alkenes is favored. Alkenes are isomerized more easily according to the HC mechanism. In all, the trends of the isomer selectivity dependent on the process conditions for the integrated process do not seem as pronounced as for the HC alone [54] – except for temperature.

As in the case of the FT reference experiments, CO conversion also affects the  $C_{10}$ - $C_{20}$  selectivity of the integrated FTS/HC process (Appendix, Fig. 10). The  $C_{10}$ - $C_{20}$  selectivity rises with increasing CO conversion up to a CO conversion of ca. 30 percent, above which the effect seems to level off. The isomer selectivity of the integrated FTS/HC process is not strongly dependent on the CO conversion.

### 3.2.2. HC catalyst deactivation

In the integrated FTS/HC process, the deactivation of the HC catalyst cannot be investigated separately. Nevertheless, we evaluated the  $C_{21+}$  selectivity of the three center points for both integration patterns as a HC catalyst deactivation measure. A deactivation of the HC catalyst may result in a lower cracking activity of all species. The differences between the  $C_{21+}$  selectivities are within 5 percentage points over the time on stream and no clear trend is emerging (center points Z1, Z2, Z3 in Fig. 6c highlighted with crosses). We did not observe significant differences between the sequential and hybrid configurations with respect to catalyst deactivation. Hence, reasonable long-term stability of the HC catalyst can be assumed.

### 3.2.3. Comparison of different catalyst bed configurations

After investigating the influence of the operating conditions on the conversion and selectivity of both, the FTS process and the two different integrated FTS/HC processes, we now compare the three processes at the same conditions. Fig. 6 shows the corrected CO conversion,  $C_{10}$ - $C_{20}$  selectivity,  $C_{21+}$  selectivity, isomer selectivity, and olefin selectivity at the test points for all three processes. For clarity, we focus on the three center points and the eight test points at a high temperature of 255 °C for the selectivities. At the test points with low temperature of 225 °C (test points 3, 4, 6, 8, 9, 11, 14, 15), the wax production was very low, resulting in greater uncertainties in data analysis, particularly for the cracking analysis. Moreover, the influence of CO conversion on  $C_{10}$ - $C_{20}$  selectivity is diminished at tests with higher temperatures and elevated CO conversion.

The CO conversion of the integrated FTS/HC process is equal to the CO conversion of the FTS reference process at low conversion levels (see Fig. 6a). At high conversion levels, the CO conversion is improved by process integration, whereby the hybrid configuration shows a more pronounced effect. The average improvement of CO conversion across all test points is 1.2% for the sequential configuration, whereas it is 8.1% for the hybrid configuration. High CO conversion of the FTS corresponds to high production of long chain hydrocarbons. The wax can accumulate in the catalyst bed, impeding the contact between syngas and FT catalyst due to limited solubility and diffusion of the syngas in the liquid long chain hydrocarbons. In the hybrid configuration, long chain hydrocarbons formed in the FTS are cracked immediately. This results in less wax in the bed, i.e. the interparticle spaces. The transport of the reactants to the catalyst and the effectiveness factor of the catalyst is improved [55]. Therefore, the CO conversion is enhanced in the hybrid configuration compared to the FTS reference. However, this explanation cannot be regarded for the comparison of the sequential bed with the reference. The reason for the improvement of CO conversion in the sequential configuration is not yet fully clear. Against the background, that the improvement is much smaller compared to the hybrid bed, it might be attributed to uncertainties due to the correction of the CO conversion.  $C_{10}$ - $C_{20}$  selectivity increases when integrating FTS and HC in one reactor compared to the FT reference experiment (see Fig. 6b). At some test points,

even the theoretical maximum  $C_{10}$ - $C_{20}$  selectivity of 40 percent of only FTS, derived from the ASF distribution, is exceeded. There is no clear trend whether the sequential or hybrid configuration shows a better performance. It is important to emphasize that from the analysis of the full product spectrum mainly ideal hydrocracking takes place under all investigated process conditions. The selectivity of the overall process towards methane and short chain hydrocarbons does not increase significantly. Information about the  $C_1$ - $C_9$  selectivity are provided in the [Supplementary Information](#). Hence, multiple cracking of long chain hydrocarbons can be excluded.

$C_{21+}$  selectivity of the overall process decreased, as expected, with the coupling of FTS and HC (see Fig. 6c). The cracking activity seems higher in the hybrid configuration than in the sequential configuration. One explanation may be based on the vapor-liquid equilibrium. In the case of the hybrid configuration, the gas/wax ratio is higher at each point of the reactor and thus the HC catalyst. This results in a higher liquid concentration of  $C_{21+}$ . This seems to overcompensate the lower residence time of long chain hydrocarbons on the HC catalyst as not all formed wax gets in contact with the whole amount of cracking catalyst. Furthermore, the difference in the cracking activity is also influenced by the water content. The acid sites of the zeolite catalyze cracking and isomerization. Water is known to negatively affect the acidity [56]. The HC catalyst has to resist a higher average water partial pressure in the sequential configuration, as water is a by-product of the FTS.

By integrating FTS and HC, the isomer selectivity increases (see Fig. 6d). Cracking is always accompanied by isomerization. More isomers are formed in the hybrid configuration compared to the sequential configuration. This is in line with the cracking activity and  $C_{21+}$  selectivity.

The olefin selectivity of the FTS reference experiment was between 20 and 30 percent. In the integrated FTS/HC experiments, the olefin selectivity was lower, demonstrating the hydrogenation function of the HC catalyst even under presence of CO (see Fig. 6e). More olefins are hydrogenated in the sequential configuration compared to the hybrid configuration. The metal site of the HC catalyst is responsible for the hydrogenation. Carbon monoxide could adsorb and block the metal sites, as already demonstrated in other studies [33,34]. The HC catalyst is exposed to a higher average CO partial pressure in the hybrid configuration compared to the sequential configuration, which is disadvantageous. A low olefin content in the synthetic fuel is desirable as it positively affects the ageing behavior of the fuel [14,57,58] and is required especially for the application of kerosene.

### 3.2.4. Proposal of elaborated catalyst configurations

When comparing the sequential catalyst configuration with the hybrid one for the integrated FTS/HC process, there is no distinctive difference of the  $C_{10}$ - $C_{20}$  selectivity. However, the hybrid catalyst configuration shows an elevated CO conversion at overall high conversion levels. We aim for a high CO conversion to increase the efficiency of the process. Besides, the isomer selectivity and olefin selectivity are clearly higher in the hybrid configuration. Technically, high isomer selectivity improves the cold flow properties of the synthetic liquid fuel, while a low olefin selectivity improves the long-term stability of the fuel. In summary, the hybrid configuration is advantageous in terms of CO conversion and isomer selectivity. The sequential configuration is advantageous in terms of olefin selectivity. The average water and CO partial pressure exposed to the HC catalyst seems to be the main influence parameters on the isomer and olefin selectivity respectively. To combine the advantages of the hybrid and the sequential catalyst bed, we suggest new catalyst bed configurations: sequential arrangement of FT catalyst followed by a hybrid mixture of FT and HC catalyst, as well as a catalyst bed with linearly decreasing amount of FT catalyst and simultaneous linearly increasing amount of HC catalyst (Fig. 7). This should lower olefin selectivity while maintaining high CO conversion and isomer selectivity. In both proposed new catalyst configurations, the HC catalyst is exposed to a lower average partial

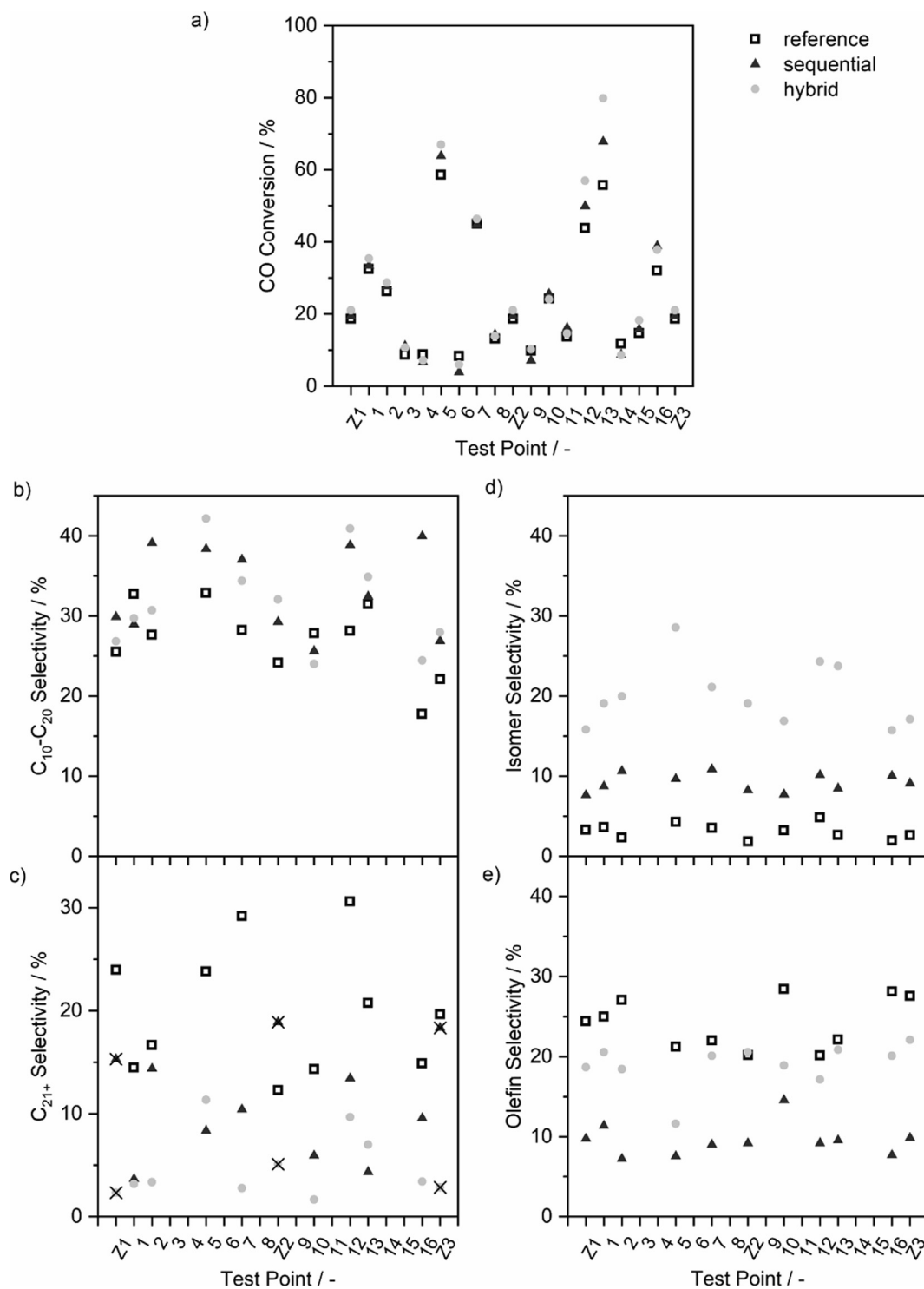


**Fig. 6.** a. CO conversion (corrected), b.  $C_{10}$ - $C_{20}$  selectivity, c.  $C_{21+}$  selectivity, d. isomer selectivity, e. olefin selectivity for the FTS reference experiment and the integrated FT/HC experiments with both, sequential and hybrid catalyst bed for different test points. For the operating conditions of each test point, please refer to [Table 2](#) and [Table 3](#). The measured  $C_{21+}$  selectivities of the three center points (marked with crosses) are a measure for the deactivation of the HC catalyst during the experiments.

pressure of CO than in the hybrid configuration. We performed basic simulation studies that lead us to suppose that with regard to the partial pressure of CO the effect of CO consumption and hydrocarbon production in the FTS outweighs the effect of decreasing  $H_2/CO$  ratio with increasing conversion of the FTS. For more information about the simulation, please refer to the [Supplementary Information](#). Moreover, the HC catalyst is exposed to a lower average partial pressure of  $H_2O$  than

in the pure sequential configuration. The mass of HC catalyst in relation to the mass of FT catalyst may also be reduced while still showing sufficient cracking of the long chain hydrocarbons. Dilution may also not be required in a microreactor.

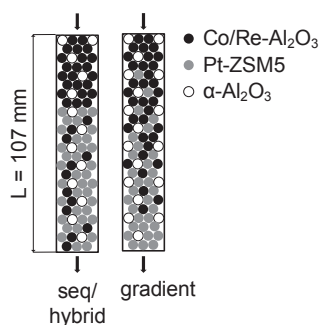


**Fig. 7.** Proposed elaborated catalyst configurations for integrated FTS/HC experiments. In the sequential/hybrid configuration (seq/hybrid) FT catalyst and a hybrid bed of FT catalyst mixed with HC catalyst are arranged in series; in the gradient configuration the amount of FT catalyst is linearly decreasing, whereas the amount of HC catalyst is linearly increasing. The catalysts are diluted with inert  $\alpha$ - $\text{Al}_2\text{O}_3$ .

#### 4. Conclusions

This experimental study shows the influence of different operation conditions such as pressure, temperature, WHSV, and  $\text{H}_2/\text{CO}$  syngas ratio on the productivity and selectivity of an integrated FTS/HC process producing synthetic liquid fuels. Going beyond existing literature studies, in addition to the chain length distribution, we also evaluated the type of produced hydrocarbons, distinguishing between n-alkanes, iso-alkanes and olefin. The type of produced hydrocarbons considerably

affects the product quality. We integrated FTS and HC at the reactor level in a single micro-structured reactor to simplify the conventional process with product separation in between FTS and HC. Process simplification is especially important for decentralized small-scale plants in context of energy transition. We investigated the integrated FTS/HC process with two different catalyst bed configurations: the sequential configuration with serial arrangement of FT and HC catalyst, and the hybrid configuration with physical mixture of both catalysts. By applying a factorial design approach, this study systematically demonstrates the effects of the considered process parameters on the target parameters such as CO conversion,  $\text{C}_{10}\text{-C}_{20}$  selectivity, isomer and olefin selectivity. The statistical planning of experiments avoids misinterpretation of the experimental data due to time-dependent phenomena such as deactivation of both catalysts over the time of the experiments. This way our study goes beyond existing literature studies. We aim for a high CO conversion and a high selectivity towards our desired product of hydrocarbons in the range of 10–20 C-atoms. At the same time, we aim for a high isomer selectivity and a low olefin selectivity to improve the cold flow properties and the stability of the fuel. This study does not investigate single effects in detail but focuses on the identification of significant process parameters for the practical application of PtL plant. To the best of our knowledge, no other study on an integrated FTS/HC process as extensive as this one has been carried out, accounting for not only the fuel selectivity, but also the product quality.

The integration of FTS and HC is beneficial, as the coupling of these two reactions facilitates a higher  $\text{C}_{10}\text{-C}_{20}$  selectivity of the overall process, and, under certain conditions, a boosted CO conversion. Moreover, the isomer selectivity increases, and the olefin selectivity

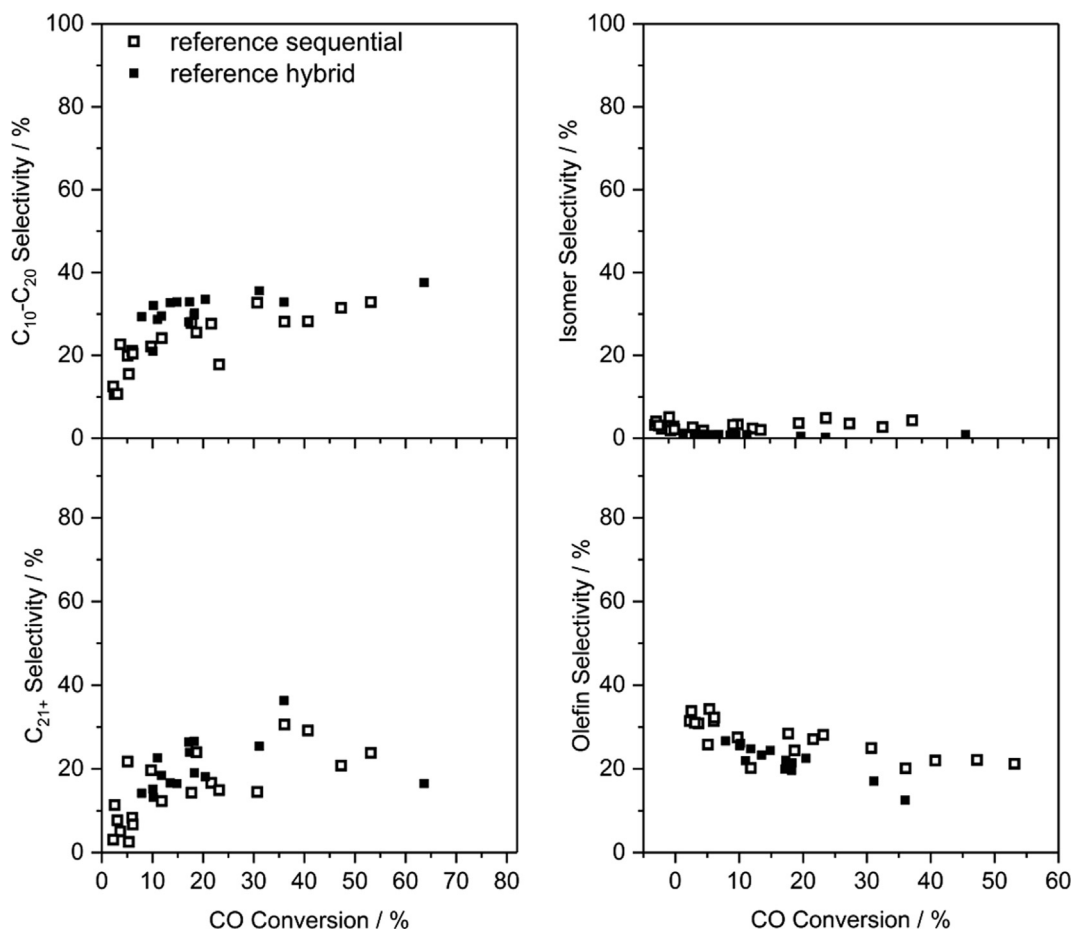


**Fig. 8.**  $\text{C}_{10}\text{-C}_{20}$  selectivity,  $\text{C}_{21+}$  selectivity, isomer selectivity, and olefin selectivity over the CO conversion for both FT reference experiments. Data is plotted over the uncorrected (time-dependent) measured CO conversion. For both FT reference experiments, the catalyst bed contained only FT catalyst mixed with inert  $\alpha$ - $\text{Al}_2\text{O}_3$ . The arranged distribution of the FT catalyst over the reactor is distinguished between sequential bed and hybrid bed arrangement.

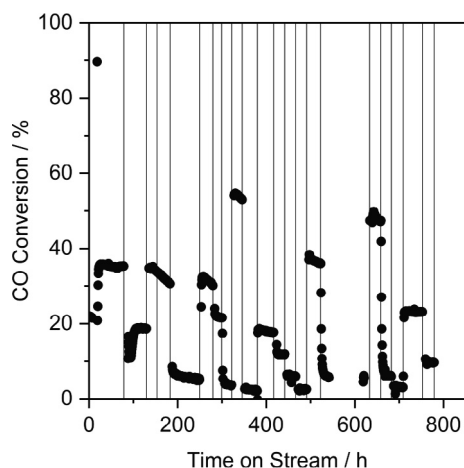


Fig. 9. CO conversion of the FT reference experiment (sequential configuration) over time on stream. Vertical lines indicate switching of operating conditions. Catalyst deactivation during test points with enhanced CO conversion is stronger. Please note, rapid change of CO conversion directly after the change of operating conditions is attributed the effect of reaction conditions on conversion combined with the inertia of the experimental plant and not to catalyst deactivation.

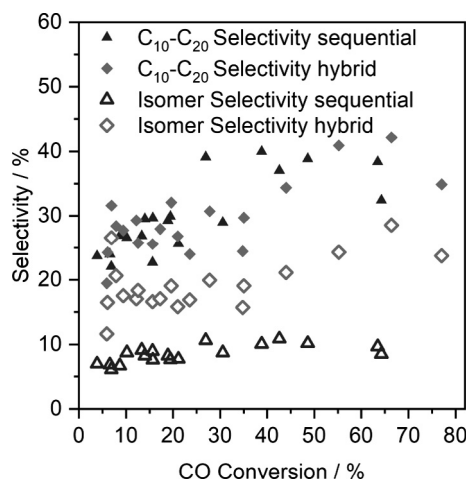


Fig. 10.  $C_{10}$ - $C_{20}$  selectivity and isomer selectivity over the CO conversion for all test points of the integrated FTS/HC experiments. Both catalyst configurations, the sequential one and the hybrid one, are shown. Data is plotted over the uncorrected (time-dependent) measured CO conversion.

decreases even under the presence of CO.

The impacts of the operating conditions on the integrated FTS/HC process are complex. The effects of the process conditions on FTS and HC could be detrimental and they do not only influence the kinetics but also the vapor-liquid equilibrium and therefore the reactor hydrodynamics. A high temperature and a low WHSV strongly improve the CO conversion and the selectivity of the integrated process towards hydrocarbons with a chain length of 10–20 C-atoms. We suggest operating PtL plants at 255 °C, the highest temperature studied. Regarding the WHSV, it exists an optimum with respect to the productivity of the integrated process. Pressure and  $H_2/CO$  syngas ratio affect CO conversion and  $C_{10}$ - $C_{20}$  selectivity only slightly. We suggest running this PtL process at 20 bar for economic considerations due to less required compression energy. Furthermore, this PtL process can easily compensate fluctuations in the synthesis gas composition – depending on the source of syngas or the availability of renewable energy – to a certain degree. In general, it is important to run the integrated FTS/HC unit at high CO conversion. Independently from the process conditions, a high CO conversion positively affects the  $C_{10}$ - $C_{20}$  selectivity. Tailor-made reactors promoting heat and mass transfer are very well suited to reach high per pass conversions. The isomer selectivity of the integrated process is not heavily affected by the operating conditions, but by the integration pattern. The integration pattern also affects the olefin selectivity. The hybrid configuration showed a higher isomer selectivity,

whereas the sequential configuration showed a lower olefin selectivity. The main reason for the influence of the integration pattern on the isomer and olefin selectivity seems the suboptimal operation conditions of the HC catalyst in the integrated FTS/HC process. The HC catalyst is exposed to water and CO. However, the stability of both catalysts under suboptimal reaction conditions of the integrated process is proven feasible. In line with existing literature studies we confirm that the hybrid configuration is advantageous over the sequential configuration in terms of cracking activity of the FT waxes. However, we would like to emphasize that the high olefin content of the liquid fuel negatively affects its quality. Therefore, we came up with elaborated catalyst configurations aiming for maximizing isomer selectivity while minimizing olefin selectivity. For practical application, we suggest focusing on a high isomer selectivity, as the crude product of PtL processes can be hydrogenated again relatively easily in case of too high olefin content. As the lower average residence time of long chain hydrocarbons on the HC catalyst in the hybrid configuration did not seem to have a dominant effect, the mass ratio of FT and HC catalyst could also be reduced.

#### Declaration of Competing Interest

The authors declare that they have no known competing financial interests or personal relationships that could have appeared to

influence the work reported in this paper.

## Acknowledgements

The authors gratefully acknowledge financial support of this work via provision of a PhD scholarship to Hannah Kirsch by the Peter und Luise Hager Foundation.

The authors would like to thank the DVGW-Forschungsstelle at

## Appendix A

## Appendix B. Supplementary data

Supplementary data to this article can be found online at <https://doi.org/10.1016/j.cej.2020.124553>.

## References

- [1] Y.N. Harari, 21 lessons for the 21st century, Jonathan Cape, London, 2018.
- [2] United Nations, Paris Agreement, 2015, <https://unfccc.int/process-and-meetings/the-paris-agreement/the-paris-agreement>, accessed 15 October 2019.
- [3] V. Masson-Delmotte, P. Zhai, H.-O. Pörtner, D. Roberts, J. Skea, P.R. Shukla, A. Pirani, W. Moufouma-Okia, C. Péan, R. Pidcock, S. Connors, J.B.R. Matthews, Y. Chen, X. Zhou, M.I. Gomis, E. Lonnoy, T. Maycock, M. Tignor, T. Waterfield, Global Warming of 1.5°C: An IPCC Special Report on the impacts of global warming of 1.5°C above pre-industrial levels and related global greenhouse gas emission pathways, in the context of strengthening the global response to the threat of climate change, sustainable development, and efforts to eradicate poverty, 2018, <https://www.ipcc.ch/sr15/download/#full>, accessed 15 October 2019.
- [4] O. Edenhofer, R. Pichs-Madruga, Y. Sokona, E. Farahani, S. Kadner, K. Seyboth, A. Adler, I. Baum, S. Brunner, P. Eickemeier, B. Kriemann, J. Savolainen, S. Schlömer, C. von Stechow, T. Zwickel, J.C. Minx, Climate Change 2014 – Mitigation of Climate Change: Working Group III Contribution to the Fifth Assessment Report of the Intergovernmental Panel on Climate Change, 2014, [https://www.ipcc.ch/site/assets/uploads/2018/02/ipcc\\_wg3\\_ar5\\_full.pdf](https://www.ipcc.ch/site/assets/uploads/2018/02/ipcc_wg3_ar5_full.pdf), accessed 15 October 2019.
- [5] European Climate Foundation (ECF), Roadmap 2050: A practical guide to a prosperous, low-carbon Europe, 2010, <https://www.roadmap2050.eu/project/roadmap-2050>, accessed 15 October 2019.
- [6] Federal Ministry for Economic Affairs and Energy (BMWi), Renewable Energy Sources in Figures: National and International Development 2017, 2018, <https://www.bmwi.de/Redaktion/EN/Publikationen/renewable-energy-sources-in-figures-2017.html>, accessed 15 October 2019.
- [7] ProcessNet-Arbeitsausschuss "Alternative flüssige und gasförmige Kraft- und Brennstoffe", Advanced alternative liquid fuels: For climate protection in the global raw materials change, 2018, [https://dechema.de/dechema\\_media/Downloads/Positionspapier/2018\\_alternativeBrennstoffe\\_en-p-20005513.pdf](https://dechema.de/dechema_media/Downloads/Positionspapier/2018_alternativeBrennstoffe_en-p-20005513.pdf), accessed 15 October 2019.
- [8] A. Goeppert, M. Czaun, G.K. Surya Prakash, G.A. Olah, Air as the renewable carbon source of the future: an overview of CO<sub>2</sub> capture from the atmosphere, *Energy Environ. Sci.* 5 (2012) 7833.
- [9] D. Cressey, Commercial boost for firms that suck carbon from air, *Nature* 526 (2015) 306–307.
- [10] A. AlNouss, G. McKay, T. Al-Ansari, Production of syngas via gasification using optimum blends of biomass, *J. Cleaner Prod.* 242 (2020) 118499.
- [11] R.C. Brown (Ed.), Thermochemical processing of biomass: Conversion into fuels, chemicals and power, Second edition ed., Wiley, Chichester, West Sussex, 2019.
- [12] G. Centi, S. Perathoner, Opportunities and prospects in the chemical recycling of carbon dioxide to fuels, *Catal. Today* 148 (2009) 191–205.
- [13] O. Posdziech, T. Geißler, K. Schwarze, R. Blumentritt, System development and demonstration of large-scale high-temperature electrolysis, *ECS Trans.* 91 (2019) 2537–2546.
- [14] A. de Klerk, Fischer-Tropsch Refining, Wiley-VCH, Weinheim, 2011.
- [15] G.P. van der LAAN, A.A.C.M. BEENACKERS, Kinetics and Selectivity of the Fischer-Tropsch Synthesis: A Literature Review, *Catalysis Reviews* 41 (1999) 255–318.
- [16] J. Weitkamp, Catalytic hydrocracking-mechanisms and versatility of the process, *ChemCatChem* 4 (2012) 292–306.
- [17] L. Kainiemi, S. Eloneva, J. Levänen, Transition towards a decentralised energy system: analysing prospects for innovation facilitation and regime destabilisation in Finland, *Technol. Anal. Strategic Manage.* 31 (2019) 1003–1015.
- [18] R. Güttel, T. Turek, Improvement of Fischer-Tropsch synthesis through structuring on different scales, *Energy Technol.* 4 (2016) 44–54.
- [19] J. Bao, G. Yang, C. Okada, Y. Yoneyama, N. Tsubaki, H-type zeolite coated iron-based multiple-functional catalyst for direct synthesis of middle isoparaffins from syngas, *Appl. Catal. A: General* 394 (2011) 195–200.
- [20] J.-C. Kim, S. Lee, K. Cho, K. Na, C. Lee, R. Ryoo, Mesoporous MFI zeolite nanopore supporting cobalt nanoparticles as a Fischer-Tropsch catalyst with high yield of branched hydrocarbons in the gasoline range, *ACS Catal.* 4 (2014) 3919–3927.
- [21] S. Sartipi, K. Parashar, M. Makkee, J. Gascon, F. Kapteijn, Breaking the Fischer-Tropsch synthesis selectivity: direct conversion of syngas to gasoline over hierarchical Co/H-ZSM-5 catalysts, *Catal. Sci. Technol.* 3 (2013) 572–575.
- [22] N. Kruse, A.G. Machoke, W. Schwieger, R. Güttel, Nanostructured encapsulated catalysts for combination of Fischer-Tropsch synthesis and hydroprocessing, *ChemCatChem* 7 (2015) 1018–1022.
- [23] A. Carvalho, M. Marinova, N. Batalha, N.R. Marcilio, A.Y. Khodakov, V.V. Ordonsky, Design of nanocomposites with cobalt encapsulated in the zeolite micropores for selective synthesis of isoparaffins in Fischer-Tropsch reaction, *Catal. Sci. Technol.* 7 (2017) 5019–5027.
- [24] A. Freitez, K. Pabst, B. Kraushaar-Czarnetzki, G. Schaub, Single-stage Fischer-Tropsch synthesis and hydroprocessing: the hydroprocessing performance of Ni/ZSM-5/γ-Al<sub>2</sub>O<sub>3</sub> under Fischer-Tropsch conditions, *Ind. Eng. Chem. Res.* 50 (2011) 13732–13741.
- [25] X. Li, K. Asami, M. Luo, K. Michiki, N. Tsubaki, K. Fujimoto, Direct synthesis of middle iso-paraffins from synthesis gas, *Catal. Today* 84 (2003) 59–65.
- [26] A. Mena Subiranas, G. Schaub, Combining Fischer-Tropsch (FT) and hydrocarbon conversion under FT reaction conditions: model compound and combined-catalyst studies, *Int. J. Chem. Reactor Eng.* 7 (2009).
- [27] K. Pabst, B. Kraushaar-Czarnetzki, G. Schaub, Combination of Fischer-Tropsch synthesis and hydroprocessing in a single-stage reactor. Part II. Effect of catalyst combinations, *Ind. Eng. Chem. Res.* 52 (2013) 8988–8995.
- [28] C. Sun, P. Pfeifer, R. Dittmeyer, One-stage syngas-to-fuel in a micro-structured reactor: investigation of integration pattern and operating conditions on the selectivity and productivity of liquid fuels, *Chem. Eng. J.* 326 (2017) 37–46.
- [29] L. Giullou, D. Balloy, P. Supiot, V. Le Courtis, Preparation of a multilayered composite catalyst for Fischer-Tropsch synthesis in a micro-chamber reactor, *Appl. Catal. A: General* 324 (2007) 42–51.
- [30] R. Myrstad, S. Eri, P. Pfeifer, E. Rytter, A. Holmen, Fischer-Tropsch synthesis in a microstructured reactor, *Catal. Today* 147 (2009) S301–S304.
- [31] P. Piermartini, T. Boeltken, M. Selinsek, P. Pfeifer, Influence of channel geometry on Fischer-Tropsch synthesis in microstructured reactors, *Chem. Eng. J.* 313 (2017) 328–335.
- [32] M. Loewert, J. Hoffmann, P. Piermartini, M. Selinsek, R. Dittmeyer, P. Pfeifer, Microstructured Fischer-Tropsch reactor scale-up and opportunities for decentralized application, *Chem. Eng. Technol.* 4 (2019) 276.
- [33] R. Brosius, J.C. Fletcher, Hydrocracking under Fischer-Tropsch conditions; the effect of CO on the mass transfer resistance by metal clusters, *J. Catal.* 317 (2014) 318–325.
- [34] N. Duyckaerts, I.-T. Trotsuş, A.-C. Swertz, F. Schüth, G. Prieto, In situ hydrocracking of Fischer-Tropsch hydrocarbons: CO-prompted diverging reaction pathways for paraffin and α-olefin primary products, *ACS Catal.* 6 (2016) 4229–4238.
- [35] S. Brunauer, L.S. Deming, W.E. Deming, E. Teller, On a theory of the van der Waals adsorption of gases, *J. Am. Chem. Soc.* 62 (1940) 1723–1732.
- [36] T.K. Das, G. Jacobs, P.M. Patterson, W.A. Conner, J. Li, B.H. Davis, Fischer-Tropsch synthesis: characterization and catalytic properties of rhenium promoted cobalt alumina catalysts, *Fuel* 82 (2003) 805–815.
- [37] T.P. Ryan, Modern experimental design, Wiley series in probability and statistics, Wiley-Interscience, Hoboken, NJ, 2007.
- [38] R. Lee, Statistical design of experiments for screening and optimization, *Chemie Ingenieur Technik* 91 (2019) 191–200.
- [39] W. Ma, G. Jacobs, Y. Ji, T. Bhatelia, D.B. Bukur, S. Khalid, B.H. Davis, Fischer-Tropsch synthesis: influence of CO conversion on selectivities, H<sub>2</sub>/CO usage ratios, and catalyst stability for a Ru promoted Co/Al<sub>2</sub>O<sub>3</sub> catalyst using a slurry phase reactor, *Top Catal.* 54 (2011) 757–767.
- [40] S. Storsæter, Ø. Borg, E.A. Blekkan, A. Holmen, Study of the effect of water on Fischer-Tropsch synthesis over supported cobalt catalysts, *J. Catal.* 231 (2005) 405–419.
- [41] J. Yang, W. Ma, D. Chen, A. Holmen, B.H. Davis, Fischer-Tropsch synthesis: a review of the effect of CO conversion on methane selectivity, *Appl. Catal. A: General* 470 (2014) 250–260.

- [42] G. Jacobs, P.M. Patterson, Y. Zhang, T. Das, J. Li, B.H. Davis, Fischer-Tropsch synthesis: deactivation of noble metal-promoted Co/Al<sub>2</sub>O<sub>3</sub> catalysts, *Appl. Catal. A: General* 233 (2002) 215–226.
- [43] H. Karaca, O.V. Safonova, S. Chambrey, P. Fongarland, P. Roussel, A. Griboval-Constant, M. Lacroix, A.Y. Khodakov, Structure and catalytic performance of Pt-promoted alumina-supported cobalt catalysts under realistic conditions of Fischer-Tropsch synthesis, *J. Catal.* 277 (2011) 14–26.
- [44] M. Sadeqzadeh, S. Chambrey, J. Hong, P. Fongarland, F. Luck, D. Curulla-Ferré, D. Schweich, J. Bousquet, A.Y. Khodakov, Effect of different reaction conditions on the deactivation of alumina-supported cobalt Fischer-Tropsch catalysts in a millifixed-bed reactor: experiments and modeling, *Ind. Eng. Chem. Res.* 53 (2014) 6913–6922.
- [45] A.M. Saib, D.J. Moodley, I.M. Ciobică, M.M. Hauman, B.H. Sigwebela, C.J. Weststrate, J.W. Niemantsverdriet, J. van de Loosdrecht, Fundamental understanding of deactivation and regeneration of cobalt Fischer-Tropsch synthesis catalysts, *Catal. Today* 154 (2010) 271–282.
- [46] N.E. Tsakoumis, M. Rønning, Ø. Borg, E. Rytter, A. Holmen, Deactivation of cobalt based Fischer-Tropsch catalysts: a review, *Catal. Today* 154 (2010) 162–182.
- [47] A.M. Hilmen, D. Schanke, K.F. Hanssen, A. Holmen, Study of the effect of water on alumina supported cobalt Fischer-Tropsch catalysts, *Appl. Catal. A: General* 186 (1999) 169–188.
- [48] G. Jacobs, T.K. Das, P.M. Patterson, J. Li, L. Sanchez, B.H. Davis, Fischer-Tropsch synthesis XAFS, *Appl. Catal. A: General* 247 (2003) 335–343.
- [49] J. Li, X. Zhan, Y. Zhang, G. Jacobs, T. Das, B.H. Davis, Fischer-Tropsch synthesis: effect of water on the deactivation of Pt promoted Co/Al<sub>2</sub>O<sub>3</sub> catalysts, *Appl. Catal. A: General* 228 (2002) 203–212.
- [50] M. Sadeqzadeh, S. Chambrey, S. Piché, P. Fongarland, F. Luck, D. Curulla-Ferré, D. Schweich, J. Bousquet, A.Y. Khodakov, Deactivation of a Co/Al<sub>2</sub>O<sub>3</sub> Fischer-Tropsch catalyst by water-induced sintering in slurry reactor: modeling and experimental investigations, *Catal. Today* 215 (2013) 52–59.
- [51] D. Schanke, A.M. Hilmen, E. Bergene, K. Kinnari, E. Rytter, E. dnanes, A. Holmen, Study of the deactivation mechanism of Al<sub>2</sub>O<sub>3</sub>-supported cobalt Fischer-Tropsch catalysts, *Catal. Lett.* 34 (1995) 269–284.
- [52] P. van Berge, J. van de Loosdrecht, S. Barradas, A. van der Kraan, Oxidation of cobalt based Fischer-Tropsch catalysts as a deactivation mechanism, *Catal. Today* 58 (2000) 321–334.
- [53] M. Wolf, E.K. Gibson, E.J. Olivier, J.H. Neethling, C.R.A. Catlow, N. Fischer, M. Claeys, Water-induced formation of cobalt-support compounds under simulated high conversion Fischer-Tropsch environment, *ACS Catal.* 9 (2019) 4902–4918.
- [54] S. Gamba, L.A. Pellegrini, V. Calemma, C. Gambaro, Liquid fuels from Fischer-Tropsch wax hydrocracking: Isomer distribution, *Catal. Today* 156 (2010) 58–64.
- [55] C. Sun, Z. Luo, A. Choudhary, P. Pfeifer, R. Dittmeyer, Influence of the condensable hydrocarbons on an integrated Fischer-Tropsch synthesis and hydrocracking process: simulation and experimental validation, *Ind. Eng. Chem. Res.* 56 (2017) 13075–13085.
- [56] A.G. Gayubo, A.T. Aguayo, A. Atutxa, R. Prieto, J. Bilbao, Role of reaction-medium water on the acidity deterioration of a HZSM-5 zeolite, *Ind. Eng. Chem. Res.* 43 (2004) 5042–5048.
- [57] R. Pereira, V. Pasa, Effect of mono-olefins and diolefins on the stability of automotive gasoline, *Fuel* 85 (2006) 1860–1865.
- [58] E.R. Strevia, V.M.D. Pasa, J.R. Sodr , Aging effects on gasoline–ethanol blend properties and composition, *Fuel* 90 (2011) 215–219.
- [59] M. Thommes, Physical adsorption characterization of nanoporous materials, *Chemie Ingenieur Technik* 82 (2010) 1059–1073.